ACS OMEGA

Article

http://pubs.acs.org/journal/acsodf

Multifunctional Biochar for Highly Efficient Capture, Identification, and Removal of Toxic Metals and Superbugs from Water Samples

Ye Gao, Avijit Pramanik, Salma Begum, Carrie Sweet, Stacy Jones, Azmain Alamgir, and Paresh Chandra Ray*

Department of Chemistry and Biochemistry, Jackson State University, 1400 J. R. Lynch Street, P.O. Box 17910, Jackson, Mississippi 39217-0510, United States

ABSTRACT: According to the World Health Organization, more than two billion people in our world use drinking water sources which are not free from pathogens and heavy metal contamination. Unsafe drinking water is responsible for the death of several millions in the 21st century. To find facile and cost-effective routes for developing multifunctional materials, which has the capability to resolve many of the challenges associated with drinking water problem, here, we report the novel design of multifunctional fluorescence-magnetic biochar with the capability for highly efficient separation, identification, and removal of pathogenic superbugs and toxic metals from environmental water samples. Details of synthesis and characterization of multifunctional biochar that exhibits very good magnetic properties and emits bright blue light owing to the quantum confinement effect are reported. In our design, biochar, a carbon-rich low-cost byproduct of naturally abundant biomass, which exhibits heterogeneous surface chemistry and strong binding affinity via oxygen-containing group on the surface, has been used to capture pathogens and toxic metals. Biochar dots (BCDs) of an average of 4 nm size with very bright photoluminescence have been developed for the identification of pathogens and toxic metals. In the current design, magnetic nanoparticles have been incorporated with BCDs which allow pathogens and toxic metals to be completely removed from water after separation by an external magnetic field. Reported results show that owing to the formation of strong complex between multifunctional biochar and cobalt(II), multifunctional biochar can be used for the selective capture and removal of Co(II) from environmental samples. Experimental data demonstrate that multifunctional biochar can be used for the highly efficient removal of methicillin-resistant *Staphylococcus aureus* (MRSA) from environmental samples. Reported results also show that melittin, an antimicrobial peptide-attached multifunctional biochar, has the capability to completely disinfect MRSA superbugs after magnetic separation. A possible mechanism for the selective separation of Co(II), as well as separation and killing of MRSA, has been discussed.

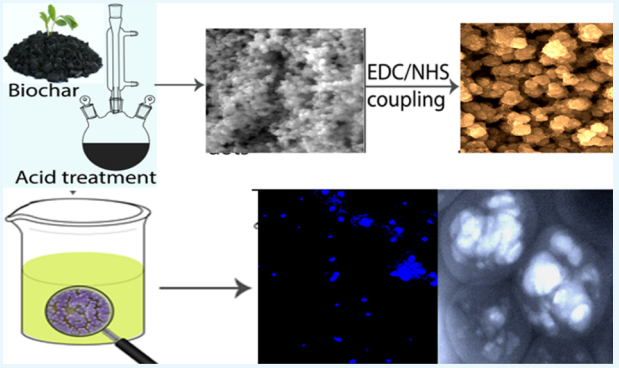

1. INTRODUCTION

As per the World Health Organization (WHO) and United Nations, by 2025, two-thirds of the population in this world will face safe drinking water shortage problems.[1−3] According to the WHO, several billions of people from Africa, Asia, and other countries have no access to clean, drinkable water which is free from toxic bacteria, virus, and heavy metals.[1−3] Unsafe drinking water is responsible for more than 10 million deaths in children under the age of five.[1−4] In the 21st century, methicillin-resistant *Staphylococcus aureus* (MRSA) superbugs, which are resistant to the conventional antibiotics, have become a nightmare for the society mainly in the USA.[5−8] A recent report also indicates that MRSA has become resistant to disinfection reagents commonly used to clean water.[7−14] Similarly, industrialization and urbanization lead to dumping of various toxic heavy metals in environmental water.[1−3] Cobalt(II) contaminates water via coal combustion and mining industry, as well as from chemical, and nuclear plant.[13−17] It is now well-documented that exposure to high concentration of cobalt can cause vasodilatation, flushing, and cardiomyopathy.[15−20] Because cobalt cannot be destroyed once it is in the environment, it is important to separate them from drinking water.[15−20] Owing to the serious water problem faced by our society now, there is a huge demand for the development of the economically viable and environmentally friendly technology which will be able to help to create a sustainable future.[1−3,7−12] Driven by the need, here, we report the development of novel multifunctional fluorescence-magnetic biochar which have the capability for separation, identification, and removal of toxic metals and superbugs from the environmental water sample, as shown in Scheme 1.

Biochar, a carbon-rich, porous solid, which can be obtained from rice husk, bean straw, corn stalk, and others, is a naturally abundant resource, which has a great potential for water

Received: September 16, 2017
Accepted: November 1, 2017
Published: November 9, 2017

DOI: 10.1021/acsomega.7b01386
ACS Omega 2017, 2, 7730−7738

Scheme 1. Multifunctional Biochar-Based Separation and Removal of Toxic Metals and Bacteria from the Environmental Water Sample

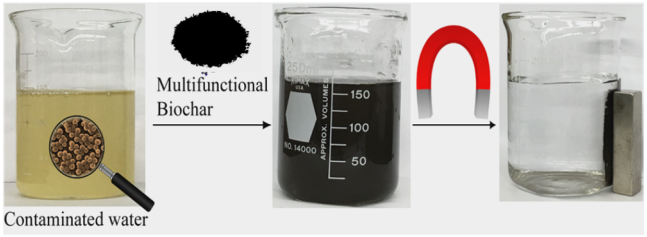

purifications.[20−30] Because biochar can be easily produced on a large scale at low cost, it has a great potential for the development of the economically viable technology for our society.[28−37] Because of the presence of abundant oxygen-containing surface functional groups such as C═O, COOH, −OH, and so forth, biochar can be used as a multifunctional platform for the capturing of toxic metals via coordination bond.[30−41] The novelty in our design is that we have developed biochar of an average size of 3 nm, which exhibits very strong photoluminescence due to quantum confinement effects. Similarly in our design, we have incorporated magnetic nanoparticles (NPs) to develop multifunctional fluorescence-magnetic biochar for targeted separation of toxic metals and pathogens from water samples. To demonstrate that multifunctional biochar can be used for the capture, identification, and removal of toxic metals and pathogens, we have used MRSA- and Co(II)-contaminated environmental samples. Experimental results show that multifunctional biochar can be used for the high-efficient capture, removal, and luminescence identification of toxic metals and superbugs from water.

Because superbug MRSA is resistant to antibiotics, we have used melittin antimicrobial peptide[42,43] (Gly-Ile-Gly-Ala-Val-Leu-Lys-Val-Leu-Thr-Thr-Gly-Leu-Pro-Ala-Leu-Ile-Ser-Trp-Ile-Lys-Arg-Lys-Arg-Gln-Gln-NH_2)-attached magnetic biochar dots (BCDs). Experimental data show that by combining melittin antimicrobial peptide with multifunctional magnetic biochar, one can separate, identify, and completely kill MRSA superbugs.

2. RESULTS ANDDISCUSSION

2.1. Development of BCDs. BCDs were synthesized from the biochar network using the hydrothermal process, as shown in Scheme 2A. In a typical procedure, 2.0 g of biochar was dispersed in a mixed solvent system of concentrated H_2SO_4 (75 mL) and concentrated HNO_3 (25 mL). The mixture was sonicated for 3 h and then oxidized by heating at 100°C for 24 h. After thermal treatment, a clear brown solution was obtained.

The solution was cooled to room temperature and diluted by adding 300 mL of double distilled water. Then, the solution was dialyzed in a 1000 D molecular weight cut-off (MWCO) dialysis membrane for 4 days. Finally, the solid BCDs were obtained by lyophilization. In the end, the solid BCDs were characterized using high-resolution scanning electron microscopy (SEM), as reported in Figure 1A and dynamic light scattering (DLS) in solution phase as reported in Table 1. Both transmission electron microscopy (TEM) and DLS measurements show that the average size is 4 nm for the BCDs we have reported here.

2.2. Development of Amino-Functionalized Magnetic NPs. The amino-functionalized magnetic NPs were synthesized

Scheme 2. (A) Synthesis Procedure Used for the Synthesis of Fluorescence BCDs from Biochar. (B) Synthesis Procedure Used for the Synthesis of Amino-Functionalized Magnetic NP from Ferrous Sulfate. (C) Synthesis Procedure Used for the Synthesis of Fluorescence-Magnetic Biochar

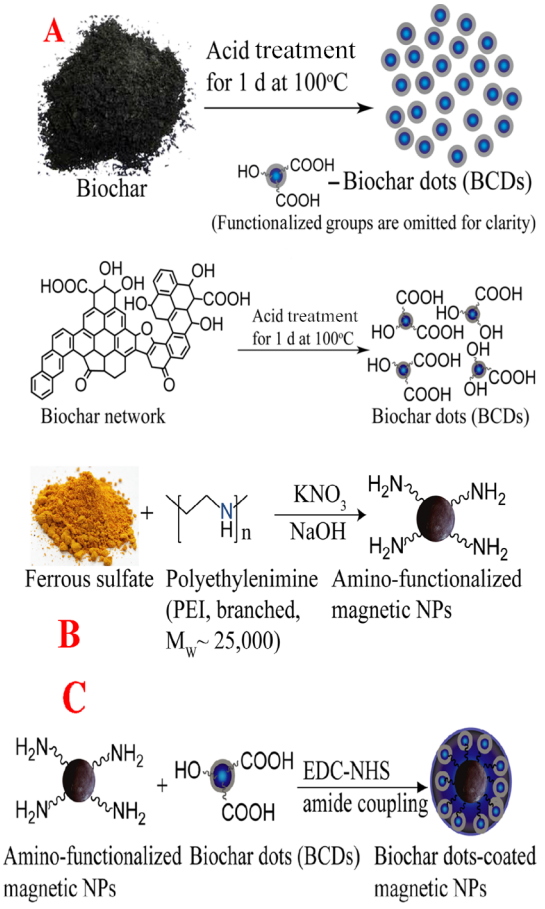

using ferrous sulfate and polyethylenimine (PEI),[44,45] as shown in Scheme 2B. For this purpose, 0.35 g of ferrous sulfate heptahydrate ($FeSO_4·7H_2O$), 5 mL of 2.0 M potassium nitrate (KNO_3), 5.0 mL of 1.0 M sodium hydroxide (NaOH), and 10 mL of 8 mg/mL PEI [branched, MW ≈ 25 000] were mixed in 40 mL of ultrapure water. The solution was purged with nitrogen for 10 min. Then, the mixture was heated to 90°C under nitrogen atmosphere with continuous stirring for 2.5 h.

The solution color was changed from blue to black, indicating the formation of iron oxide magnetic NPs. The amino-functionalized magnetic NPs were separated and purified by magnetic separation and redispersed in ultrapure water for several cycles and then dried in vacuum for few days to yield a black powder. In the end, we have used high-resolution TEM-2100F, to characterize magnetic NPs, as reported in Figure 1B. Magnetic NPs were also characterized using DLS in solution phase as reported in Table 1. Both TEM and DLS measurements show that the average size is 30 nm for the amine-functionalized magnetic NPs. We have used a SQUID magnetometer for the measurement of superparamagnetic properties, and this indicates a specific saturation magnetization of 39.6 emu g^{-1} for the amine-functionalized magnetic NPs we have synthesized.

2.3. Synthesis of BCD-Coated Magnetic NPs. We have developed BCD-coated magnetic NPs via functionalization of

DOI: 10.1021/acsomega.7b01386
ACS Omega 2017, 2, 7730−7738

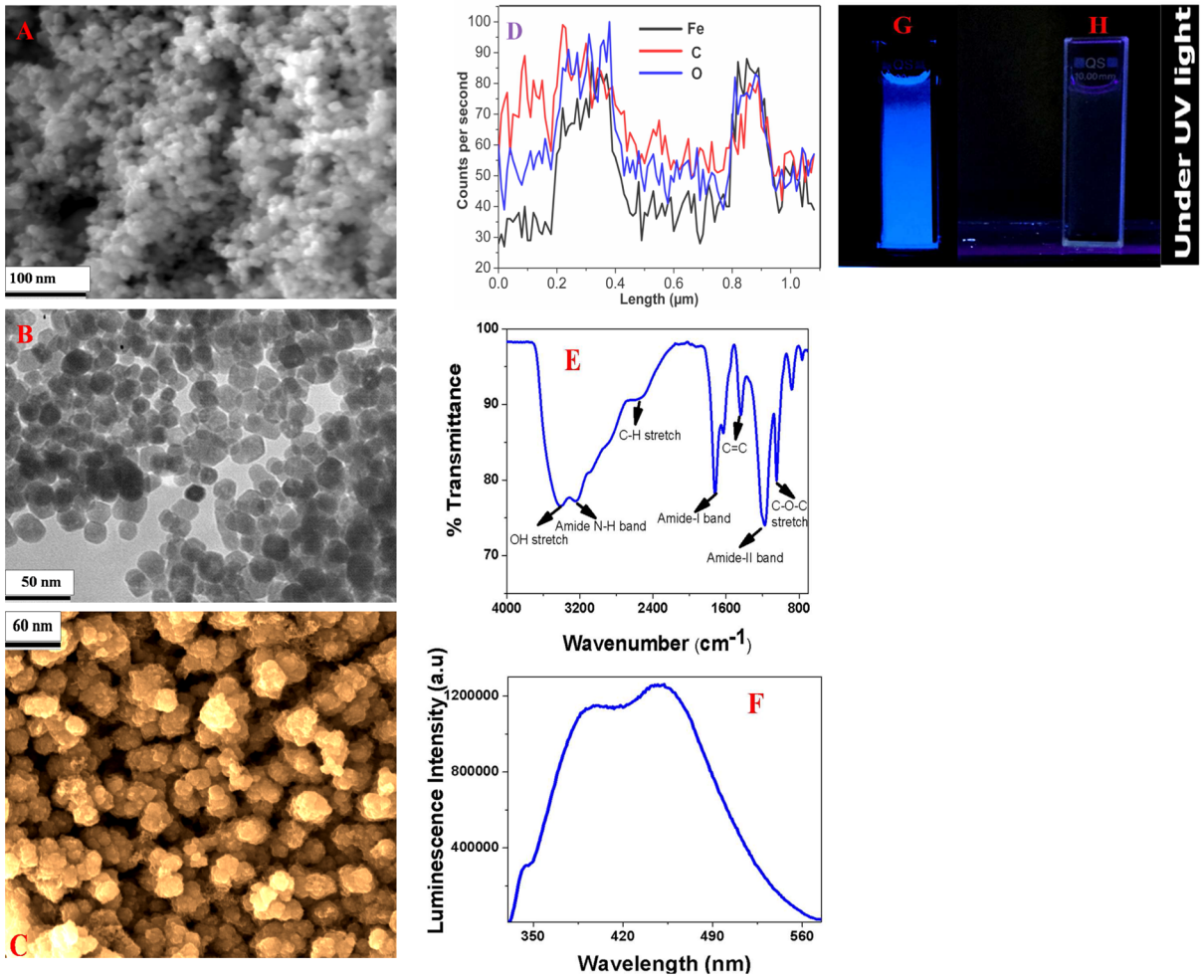

Figure 1. (A) High-resolution SEM image of freshly synthesized BCDs. (B) High-resolution TEM image of freshly synthesized amino-functionalized magnetic NPs. (C) High-resolution SEM image of the BCD-coated magnetic NPs. (D) Energy-dispersive X-ray (EDX) mapping data from the freshly synthesized BCD-coated magnetic NPs show the presence of Fe, C, and O in the BCD-coated magnetic NPs. (E) Fourier transform infrared (FTIR) spectrum from freshly synthesized BCD-coated magnetic NPs shows the existence of amide NH, amide-I and II, C−O−C, CO, −OH, and−C−OH groups. (F) Luminescence spectra from the freshly synthesized BCD-coated magnetic NP at 305 nm excitation, which indicate that luminescence λ_{max} is around 460 nm. (G) Fluorescence under 305 nm UV light clearly shows that freshly synthesized BCD-coated magnetic NPs emit green fluorescence when excited by UV light. (H) Fluorescence under 305 nm UV light clearly shows that the freshly synthesized cubic-shaped magnetic NPs does not emit any fluorescence when excited by the UV light.

Table 1. Size Distribution for BCDs, Amine-Functionalized Magnetic NPs, and Multifunctional Fluorescence-Magnetic Biochar Measured by DLS and SEM/TEM Techniques

nanosystem description	size measured by DLS (nm)	size measured by TEM/SEM (nm)
BCDs	4 ± 2	4 ± 2
amine-functionalized magnetic NP	25± 5	25± 8
multifunctional biochar	40±12	40± 10

amino-functionalized magnetic NPs with water soluble BCDs, as shown in Scheme 2C. BCD-coated magnetic NPs are developed by coupling the $-CO_2H$ of BCDs with the amine group of PEG in the presence of 1-ethyl-3-(3-dimethylaminopropyl)carbodiimide (EDC) cross-linking agent. For this purpose, 5.0 mg of BCDs and 5.0 mg of amino-functionalized magnetic NPs were each dissolved in 3 mL of phosphate buffer separately. The BCD solution was then mixed with 2 mL of 0.2 M EDC and 0.05 M *N*-hydroxysulfosuccinimide sodium salt [1:3 (v/v) ratio] for the activation of −COOH group present in BCDs solution under constant stirring. The yield was 80%.

After 20 min, 3 mL of amino-functionalized magnetic NPs was added dropwise into the activated BCD solution. The final mixture was vortexed overnight. Then, the reaction mixture was dialyzed for 2 days in a 2000 MWCO dialysis tubing to remove excess reactants, and the purified BCD-coated magnetic NPs were characterized using high-resolution SEM, EDX spectroscopy, infrared spectroscopy, and luminescence and absorption spectroscopy, as reported in Figure 1C−H. Multifunctional biochar was also characterized using DLS in solution phase as reported in Table 1.

2.4. Characterization of Multifunctional Biochar. Figure 1C shows the high-resolution SEM image of BCD-coated magnetic NPs, which indicates that the particle size of multifunctional biochar is about 40 nm. DLS measurement in solution phase, as reported in Table 1, also shows that the particle size of the freshly prepared multifunctional biochar is about 40 nm. The EDX mapping data from the freshly prepared multifunctional biochar, as reported in Figure 1D, show the

DOI: 10.1021/acsomega.7b01386
ACS Omega 2017, 2, 7730−7738

presence of Fe, C, and O, indicating the presence of iron oxide NPs in multifunctional biochar. Figure 1E shows the FTIR data from the freshly prepared multifunctional biochar, which clearly indicates the presence of amide-A band, amide-I bands, and amide-II band, which indicate the formation of amide linkage between CO_2H-functionalized biochar and amine-functionalized magnetic NPs. In the FTIR spectra of the freshly prepared multifunctional biochar, we have also observed OH stretching band, C−H stretching band, C═C band, and C−O−C stretching bands, as reported in Figure 1E. Figure 1F shows the luminescence spectra of the freshly prepared multifunctional biochar with λ_{max} at 460 nm. Figure 1G shows that water soluble multifunctional biochar emits blue color fluorescence upon the irradiation of UV light. On the other hand, only magnetic NPs do not exhibit any fluorescence upon the irradiation of UV light. We have also measured photoluminescence quantum yield (QY) for multifunctional fluorescence-magnetic biochar, using quinine sulfate as a standard (Φ = 54%). The QY for multifunctional biochar was determined to be 16.8%. We have used a SQUID magnetometer for the measurement of superparamagnetic properties of the fluorescence-magnetic multifunctional biochar, and it shows a specific saturation magnetization of 34.4 emu g^{-1} for multifunctional biochar, as synthesized.

2.5. Capture and Identification of Cobalt(II) from the Infected Water Sample. Next, to understand whether our multifunctional biochar can be used for the separation and identification of Co(II) from the water sample, we have infected 100 mL of the water sample using different concentrations of cobalt(II). After that, we have incubated 1 mg of multifunctional biochar with 100 mL of Co(II)-infected water sample. After 30 min of incubation, we have used a bar magnet to capture and remove Co(II) from the infected water sample, as shown in Scheme 1. As shown in Scheme 3, because Co(II) can form bis(biochar dots)cobalt(II) complex and tris(biochar dots)cobalt(II) complex, during the magnetic separation, multifunctional biochar−Co(II) complex was magnetically separated and removed from the water sample. After that, we have used inductively coupled plasma mass spectrometry to determine the concentration of Co(II) in the supernatant and the magnetically separated part.

As reported in Figure 2A and Table 1, our experimental data clearly show that more than 97% of Co(II) has been captured and removed by multifunctional biochar. On the other hand, less than 10% of Co(II) was removed when only magnetic NPs was used, which clearly indicates that multifunctional biochar is highly novel for the separation of cobalt(II) from environmental samples. The observed very high removal efficiency of Co(II) using multifunctional biochar is mainly due to the fact that cobalt(II) is known to have very high binding with carboxylic acid and catechol, via the formation of bis and tris complex as shown in Scheme 2. It is also reported that the binding constant between cobalt(II) and carboxylic acid is higher than that of Pb(II), Cd(II), Fe(III), and so forth. To understand better, we have also performed a photoluminescence measurement in the presence and absence of cobalt(II). We have used 305 nm excitation light for this experiment. As reported in Figure 2C, more than 95% luminescence at λ_{max} 460 nm was quenched in the presence of cobalt(II). It is mainly due to the formation of nonluminescence bis(biochar dots)cobalt(II) complex and tris(biochar dots)cobalt(II) complex, as shown in Scheme 2.

Scheme 3. (A,C) Possible Formation of Bis(BCDs) Cobalt(II) Complex via the Interaction between Co(II) and Multifunctional Biochar. (B) Possible Formation of Tris(BCDs) Cobalt(II) Complex via the Interaction between Co(II) and Multifunctional Biochar

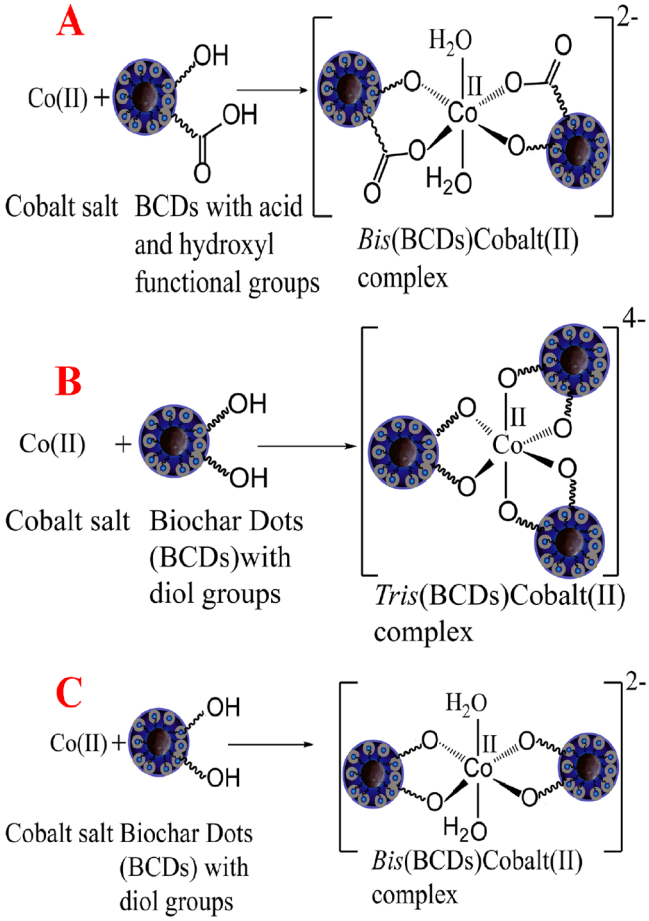

Figure 2D shows how the quenching efficiency depends on the concentration of Co(II). Reported result clearly shows that the quenching efficiency is highly dependent on the concentration of Co(II). Concentration-dependent quenching efficiency data, as reported in Figure 2D, indicate that multifunctional biochar luminescence quenching-based method can be used for the detection of Co(II) in the water sample even at the concentration of 1 ppb.

To understand how selective is the bonding between multifunctional biochar and Co(II), we have performed the same experiment using other heavy metal ions such as Pb(II), Zn(II), Cr(III), Fe(III), Hg(II), and As(III). As reported in Figure 2F,G, experimental data show that less than 20% of other heavy metal ions such as Pb(II), Zn(II), Cr(III), Fe(III), Hg(II), and As(III) were captured and separated using multifunctional biochar, whereas more than 97% Co(II) were captured and removed by multifunctional biochar. All of the above data clearly show that the designed novel multifunctional biochar can be used for the selective capture and removal of Co(II) from the water sample. Because multifunctional biochar is selective for Co(II), to find out whether multifunctional biochar can be used for the capture and separation of Co(II) from the environmental water sample, we have collected water samples from Mississippi Reservoir and Mississippi River and contaminated it by Co(II). As shown in Figure 2A, the removal

DOI: 10.1021/acsomega.7b01386
ACS Omega 2017, 2, 7730−7738

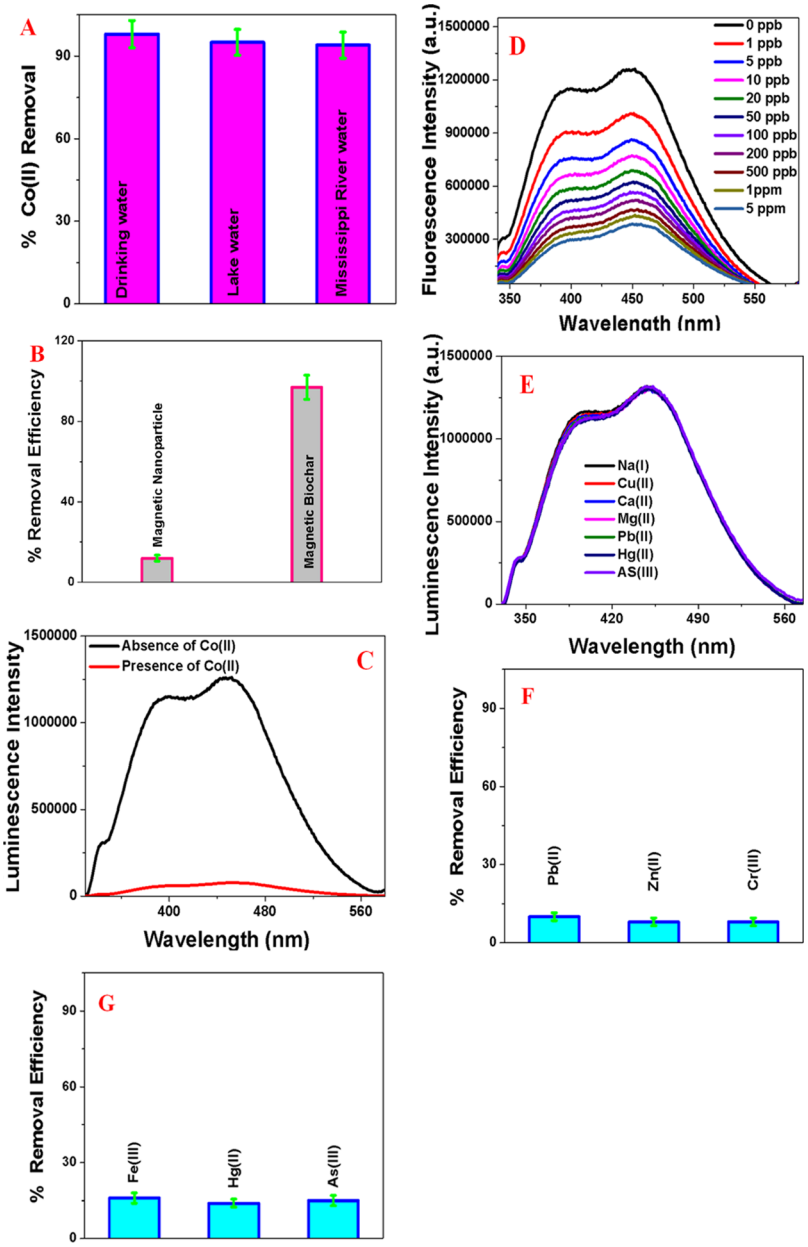

Figure 2. (A) Cobalt(II) removal efficiency from environmental water samples using multifunctional magnetic biochar. (B) Comparison of the cobalt(II) removal efficiency from the water sample using magnetic NP and multifunctional magnetic biochar. (C) Plot shows that the luminescence intensity from multifunctional biochar was quenched by about 95% in the presence of cobalt(II) and is mainly due to the formation of bis and tris Co(II) complex. 305 nm excitation light was used for this experiment. (D) Plot shows that multifunctional biochar luminescence can be used for the detection of Co(II) as low as 1 ppb concentration. 305 nm excitation light was used for this experiment. (E) Plot showing the luminescence intensity with λ_{max} at 460 nm from multifunctional biochar was quenched to less than 5% in the presence of other heavy metal ions such as Pb(II), Zn(II), Cr(III), Fe(III), Hg(II), and As(III). (F) Removal efficiency of Pb(II), Zn(II), and Cr(III) using multifunctional magnetic biochar. (G) Removal efficiency of Fe(III), Hg(II), and As(III) using multifunctional magnetic biochar.

efficiency of Co(II) from the environmental water sample is about the same as that we have observed in the case of drinking water.

2.6. Capture, Identification, and Killing of MRSA Superbugs Using Anti-MRSA Antibody-Attached Magnetic Biochar. For selective capture, identification, and killing of MRSA superbugs, we have developed anti-MRSA antibody-attached multifunctional biochar, as shown in Figure 3A. For the development of anti-MRSA antibody-attached multifunctional biochar, we have used the coupling chemistry between $-CO_2H$ group of multifunctional biochar and amine group of anti-*MRSA antibody* via EDC coupling, as shown in Figure 3A. After that, anti-MRSA antibody-attached biochar has been used for the separation of MRSA superbugs from the water sample. For this purpose, we have prepared an MRSA-infected sample containing 4.3×10^5 colony-forming unit (cfu)/mL of MRSA superbugs.

After the capture and separation of anti-MRSA antibody-attached multifunctional biochar, we have used the RT-PCR[49,50] technique to find out the percentage of MRSA superbugs that were separated and captured by anti-MRSA antibody-attached multifunctional biochar. We have also used

DOI: 10.1021/acsomega.7b01386
ACS Omega 2017, 2, 7730−7738

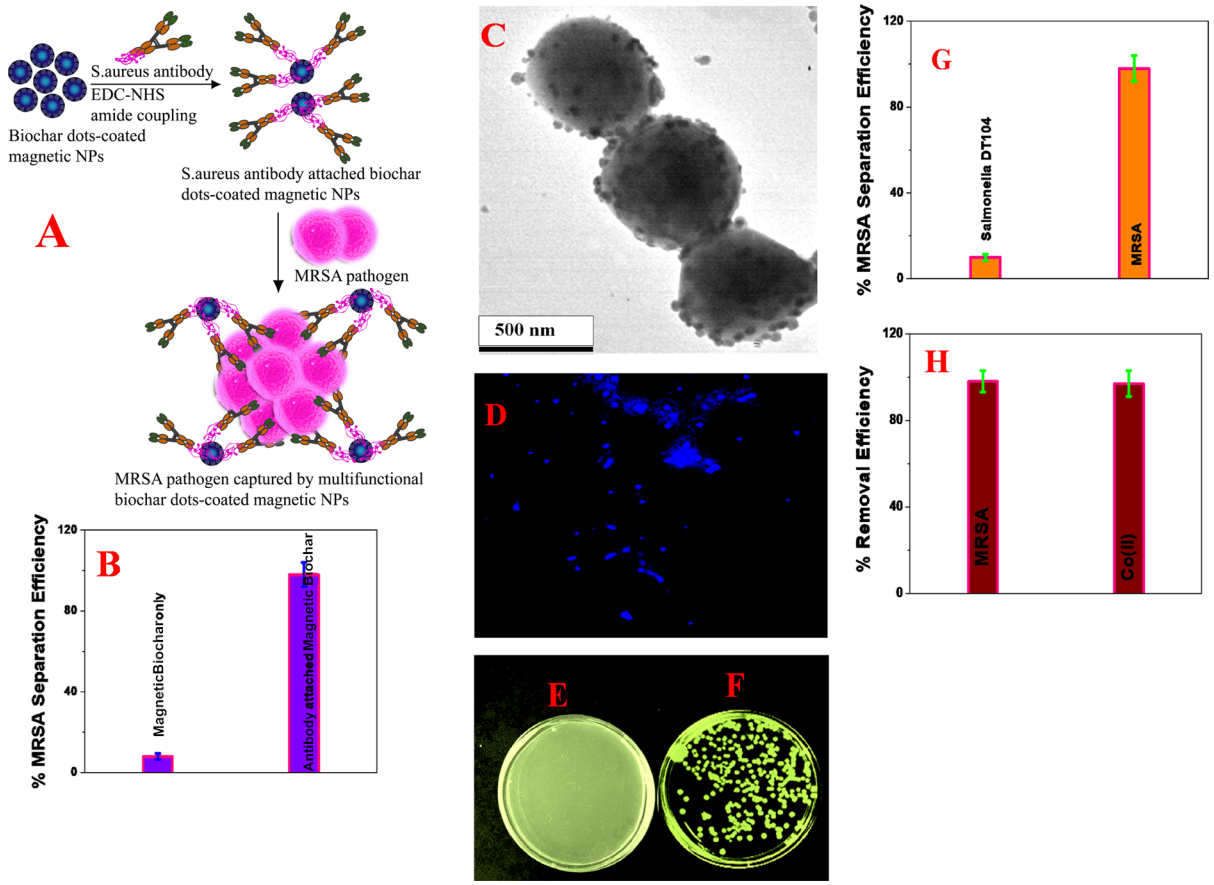

Figure 3. (A) Schematic representation showing the synthetic scheme we have used to develop anti-MRSA antibody-attached multifunctional biochar. (B) Comparison of the MRSA superbug removal efficiency from the water sample using magnetic NPs and anti-MRSA antibody-attached multifunctional biochar. We have used the reverse-transcription polymerase chain reaction (RT-PCR) to find out the percentage of MRSA superbugs that were separated. (C) TEM image of MRSA superbugs captured by anti-MRSA antibody-attached multifunctional biochar. (D) Fluorescence image of the MRSA superbugs captured by anti-MRSA antibody-attached multifunctional biochar. (E,F) Colony-counting of MRSA, (E) after magnetic separation using anti-MRSA antibody-attached multifunctional biochar and (F) after magnetic separation using magnetic biochar without antibody. (G) Plot shows the selectivity of MRSA superbug removal using anti-MRSA antibody-attached multifunctional biochar. (H) Plots show the removal efficiency of MRSA superbug and Co(II) heavy metal simultaneously from the infected water sample using anti-MRSA antibody-attached multifunctional biochar.

TEM and fluorescence microscope images to characterize the MRSA superbugs captured by anti-MRSA antibody-attached multifunctional biochar. As reported in Figure 3B and Table 2,

Table 2. Separation Efficiency of Cobalt(II) and MRSA, as well as Killing Efficiency of MRSA Using Magnetic NP and Multifunctional Biochar

nanosystem description	% cobalt(II) removal efficiency	% MRSA separation and killing efficiency
magnetic NP	10 ± 2	25 ± 8
multifunctional biochar	12 ± 3	100 ± 5

the RT-PCR data indicate that multifunctional biochar is able to remove around 100% of MRSA superbugs from the infected water sample. Similarly, the colony-counting data, reported in Figure 3E,F, also confirm the RT-PCR data. The TEM image (Figure 3C)clearly shows that the MRSA superbugs are attached with anti-MRSA antibody-attached multifunctional biochar, and as a result, these superbugs are captured and separated by the magnet.

The fluorescence image (Figure 3D) shows that the MRSA superbugs are attached with the anti-MRSA antibody-attached multifunctional biochar, and as a result, these superbugs can be viewed in the fluorescence image after being separated by a magnet. This highly efficient MRSA superbug removal using the anti-MRSA antibody-attached multifunctional biochar is mainly due to the antigen−antibody interaction which allows 100% of MRSA superbugs to attach with the anti-MRSA antibody-attached multifunctional biochar and can be separated by a magnet. To understand better, we have also performed the same experiment using multifunctional biochar in the absence of anti-MRSA antibody. As reported in Figure 3B, reported RT-PCR data clearly indicate that the presence of anti-MRSA antibody is highly necessary for the efficient removal of MRSA superbugs using multifunctional biochar. To understand how selective the removal efficiency for MRSA superbugs is using anti-MRSA antibody-attached multifunctional biochar, we have performed the same removal experiment using *Salmonella DT104* bacteria. For this purpose, we have used 4.3×10^5 cfu/mL *Salmonella DT104* bacteria. As reported in Figure 3G, our experimental data clearly indicate that the anti-MRSA antibody-attached multifunctional biochar developed by us is selective for the removal of MRSA superbugs from the infected water sample. Because the environmental sample can contain both toxic metals and pathogens together, to understand whether

DOI: 10.1021/acsomega.7b01386
ACS Omega 2017, 2, 7730−7738

anti-MRSA antibody-attached multifunctional biochar developed by us can be used for the separation of Co(II) and *MRSA* superbugs simultaneously, we have collected a water sample from the Mississippi River and infected the water by Co(II) and *MRSA* superbugs simultaneously. As reported in Figure 3H, anti-MRSA antibody-attached multifunctional biochar can be used for the high-efficient removal of Co(II) and MRSA superbugs simultaneously from the environmental water sample.

Because MRSA is a drug-resistant and contagious pathogen, MRSA needs to be inactivated after separation, before it can spread in the society.[1−5] For this purpose, we have developed a melittin antimicrobial peptide[42,43] (Gly-Ile-Gly-Ala-Val-Leu-Lys-Val-Leu-Thr-Thr-Gly-Leu-Pro-Ala-Leu-Ile-Ser-Trp-Ile-Lys-Arg-Lys-Arg-Gln-Gln-NH_2)-attached multifunctional magnetic BCDs. For developing the melittin antimicrobial peptide-attached multifunctional biochar, the coupling chemistry between $-CO_2H$ group of multifunctional biochar and the amine group of melittin antimicrobial peptide has been used via EDC coupling. To find out the antimicrobial activity for our melittin antimicrobial peptide-attached multifunctional biochar, after magnetic separation of MRSA using melittin antimicrobial peptide-attached multifunctional biochar, we have used the colony-plating technique to determine the amount of live *MRSA*.

Figure 4A−D and Table 2 clearly show that 100% MRSA superbugs were killed after they were separated by melittin antimicrobial peptide-attached multifunctional biochar. On the other hand, less than 5% of MRSA were killed when only magnetic NPs were used, which clearly indicates that multifunctional biochar is highly novel for the separation and killing of MRSA from the environmental sample. Very high antimicrobial activity has been observed in the presence of melittin antimicrobial peptide-attached multifunctional biochar, which is due to possible formation of pores on the MRSA membrane.[42,43] A honeybee venom-derived antimicrobial peptide, named melittin, has been used as the antimicrobial peptide that can induce pores on MRSA membranes.[42,43] It is now well-documented that when melittin has been used in the nanomolar range, it has the capability to induce transient pores via leakage of glucose or larger molecules.[42,43] It has been reported that when micromolar concentrations have been used, melittin induces stable pore formation which allows antimicrobial activities.[42,43] To understand the possible pore formation by melittin antimicrobial peptide-attached multifunctional biochar on the MRSA membrane, we have performed a high-resolution TEM experiment, as reported in Figure 4D. Our reported result clearly shows that melittin antimicrobial peptide-attached multifunctional biochar makes pores on the MRSA membrane and as a result, all MRSA superbugs were killed. All of the reported data clearly indicate that the novel multifunctional biochar has the capability to completely disinfect MRSA superbugs after magnetic separation.

3. CONCLUSIONS

In conclusion, we have reported the development of novel multifunctional fluorescence-magnetic biochar with the capability of highly efficient separation, identification, and removal of pathogenic superbug and toxic metals from environmental water samples. In our design of multifunctional biochar, we have used 3 nm sized, very strong photoluminescent biochar for the detection of MRSA superbugs and Co(II) toxic metals after capture using magnetic core NPs. Reported data show that

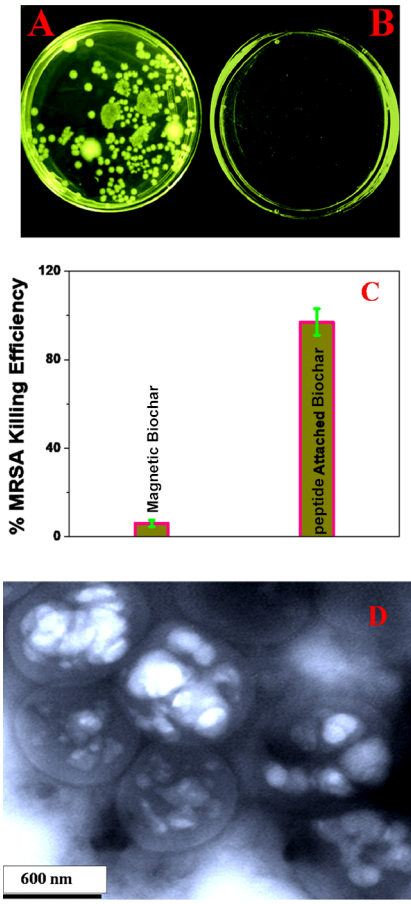

Figure 4. (A,B) MRSA killing efficiency measured using the colony-counting technique, (A) using magnetic multifunctional biochar without melittin antimicrobial peptide and (B) using melittin antimicrobial peptide-attached multifunctional biochar. (C) Comparison of the MRSA superbug killing efficiency using magnetic multifunctional biochar without melittin antimicrobial peptide and melittin antimicrobial peptide-attached multifunctional biochar. (D) TEM image clearly shows the pore formation on the surface of MRSA superbugs when the superbugs were captured by melittin antimicrobial peptide-attached multifunctional biochar.

because Co(II) can form strong complex with Co(II), more than 97% of Co(II) can be captured and separated selectively using multifunctional biochar. Strong nonluminescence complex formation between Co(II) and multifunctional biochar has been demonstrated using the luminescence quenching experiment. Reported data show that more than 95% luminescence was quenched in the presence of cobalt(II), and the complex formation is quite selective for Co(II).

Reported experimental data demonstrated that anti-MRSA antibody-attached multifunctional biochar can be used for the selective capture and separation of MRSA from the water sample. We have shown that anti-MRSA antibody-attached multifunctional biochar has the capability to separate and capture Co(II) and MRSA simultaneously from the environmental sample. The experimental result reported in this manuscript demonstrated that melittin antimicrobial peptide-attached multifunctional biochar has the capability to kill 100% MRSA via the formation of pores on the MRSA membrane. Our reported data show that multifunctional biochar development opens a new possibility for capture and removal of MRSA and Co(II) from environmental samples. Although our

DOI: 10.1021/acsomega.7b01386
ACS Omega 2017, 2, 7730−7738

reported data seem very promising, extensive research needs to be performed to find large-scale development of multifunctional biochar, and enormous attention needs to be given for the design of new ways to improve the long-term performance.

4. EXPERIMENTAL SECTION

4.1. Materials. Biochar was purchased from Amazon, US Bio Carbon 6C soil. All other chemicals such as ferrous sulfate, PEI, KNO_3, NaOH, $KMnO_4$, EDC, nitric acid, Co(II), and other heavy metal salts were purchased from Fisher Scientific and Sigma-Aldrich. MRSA superbugs and the growth media for MRSA were purchased from the American Type Culture Collection (ATCC, Rockville, MD).

4.2. MRSA Superbugs Sample Preparation. Superbugs MRSA were purchased from ATCC; then, we have cultured the superbugs according to the protocol we have reported before.[46−48] In the end, we have varied the concentration of superbugs from 5 to 10^5cfu/mL using water.

4.3. Finding the Percentage of Superbugs Captured and Separated. To determine the amount of MRSA superbugs captured by multifunctional biochar, we have used a colony-countable plate. For this purpose, after capture and removal by multifunctional biochars, we transferred the superbugs to colony-countable plates and then incubated them for a day. After that, the colony number was counted with a colony counter.

AUTHOR INFORMATION

Corresponding Author

*E-mail: paresh.c.ray@jsums.edu. Fax: +16019793674 (P.C.R.).

ORCID

Paresh Chandra Ray: 0000-0001-5398-9930

Notes

The authors declare no competing financial interest.

ACKNOWLEDGMENTS

P.C.R. thanks NSF-RII-EPSCoRgrant #1632899 and NSF-PREM grant #DMR-1205194 for their generous funding.

REFERENCES

(1) http://www.who.int/topics/drinking_water/en/ (date of access August 12, 2017).

(2) http://www.un.org/waterforlifedecade/scarcity.shtml (accessed August 17, 2017).

(3) http://water.org/water-crisis/one-billion-affected/ (date of access August 17, 2017).

(4) Rizzo, L.; Manaia, C.; Merlin, C.; Schwartz, T.; Dagot, C.; Ploy, M. C.; Michael, I.; Fatta-Kassinos, D. Urban wastewater treatment plants as hotspots for antibiotic resistant bacteria and genes spreadinto the environment: A review. *Sci. Total Environ.* **2013**, *447*, 345−360.

(5) Berendonk, T.U.; Manaia, C.M.; Merlin, C.; Fatta-Kassinos, D.; Cytryn, E.; Walsh, F.; Bürgmann, H.; Sørum, H.; Norström, M.; Pons, M.-N.; Kreuzinger, N.; Huovinen, P.; Stefani, S.; Schwartz, T.; Kisand, V.; Baquero, F.; Martinez, J. L. Tackling antibiotic resistance: the environmental framework. *Nat. Rev. Microbiol.* **2015**, *13*, 310−317.

(6) Zou, X.; Zhang, L.; Wang, Z.; Luo, Y. Mechanisms of The Antimicrobial Activities of Graphene Materials. *J. Am. Chem. Soc.* **2016**, *138*, 2064−2077.

(7) Nathan, C.; Cars, O. Antibiotic resistance—problems, progress, and prospects. *N. Engl. J. Med.* **2014**, *371*, 1761−1763.

(8) Antibiotic resistance threats in USA. www.cdc.gov/drugresistance/about.html (accessed August 17, 2017).

(9) Nellore, B. P. V.; Kanchanapally, R.; Pedraza, F.; Sinha, S. S.; Pramanik, A.; Hamme, A. T.; Arslan, Z.; Sardar, D.; Ray, P. C. Bio-Conjugated CNT-Bridged 3D Porous Graphene Oxide Membrane for Highly Efficient Disinfection of Pathogenic Bacteria and Removal of Toxic Metals from Water. *ACS Appl. Mater. Interfaces* **2015**, *7*, 19210−19218.

(10) https://www.cdc.gov/niosh/topics/mrsa/ (date of access August 12, 2017).

(11) https://www.cdc.gov/niosh/ipcsneng/neng0783.html (date of access August 12, 2017).

(12) Mural, P. K. S.; Kumar, B.; Madras, G.; Bose, S. Chitosan Immobilized Porous Polyolefin As Sustainable and Efficient Antibacterial Membranes. *ACS Sustainable Chem. Eng.* **2016**, *4*, 862−870.

(13) Sinha, S. S.; Jones, S.; Pramanik, A.; Ray, P. C. Nanoarchitecture Based SERS for Biomolecular Fingerprinting and Label-Free Disease Markers Diagnosis. *Acc. Chem. Res.* **2016**, *49*, 2725−2735.

(14) Fan, Z.; Yust, B.; Nellore, B. P. V.; Sinha, S. S.; Kanchanapally, R.; Crouch, R. A.; Pramanik, A.; Chavva, S. R.; Sardar, D.; Ray, P. C. Accurate Identification and Selective Removal of Rotavirus Using a Plasmonic−Magnetic 3D Graphene Oxide Architecture. *J. Phys. Chem. Lett.* **2014**, *5*, 3216−3221.

(15) Ryu, H.-W.; Lee, D.H.; Won, H.-R.; Kim, K. H.; Seong, Y. J.; Kwon, S. H. Influence of toxicologically relevant metals on human epigenetic regulation. *Toxicol. Res.* **2015**, *31*, 1−9.

(16) Au-Yeung, H. Y.; New, E. J.; Chang, C. J. A Selective Reaction-Based Fluorescent Probe for Detecting Cobalt in Living Cells. *Chem. Commun.* **2012**, *48*, 5268−5270.

(17) Xing, K.; Fan, R.; Wang, J.; Zhang, S.; Feng, K.; Du, X.; Song, Y.; Wang, P.; Yang, Y. Highly Stable and Regenerative Metal−Organic Framework Designed by Multiwalled Divider Installation Strategy for Detection of Co(II) Ions and Organic Aromatics in Water. *ACS Appl. Mater. Interfaces* **2017**, *9*, 19881−19893.

(18) Zhang, Z.; Chen, Z.; Pan, D.; Chen, L. Fenton-like Reaction-Mediated Etching of Gold Nanorods for Visual Detection of Co^{2+}. *Langmuir* **2015**, *31*, 643−650.

(19) Sharma, H.; Singh, A.; Kaur, N.; Singh, N. ZnO-Based Imine-Linked Coupled Biocompatible Chemosensor for Nanomolar Detection of Co2+. *ACS Sustainable Chem. Eng.* **2013**, *1*, 1600−1608.

(20) Tsoutsi, D.; Guerrini, L.; Hermida-Ramon, J. M.; Giannini, V.; Liz-Marzán, L. M.; Wei, A.; Alvarez-Puebla, R. A. Simultaneous SERS Detection of Copper and Cobalt at Ultratrace Levels. *Nanoscale* **2013**, *5*, 5841−5846.

(21) Smith, C. R.; Buzan, E. M.; Lee, J. W. Potential impact of biochar water-extractable substances on environmental sustainability. *ACS Sustainable Chem. Eng.* **2013**, *1*, 118−126.

(22) Liu, W.-J.; Jiang, H.; Yu, H.-Q. Development of Biochar-Based Functional Materials: Toward a Sustainable Platform Carbon Material. *Chem. Rev.* **2015**, *115*, 12251−12285.

(23) Hale, S. E.; Lehmann, J.; Rutherford, D.; Zimmerman, A. R.; Bachmann, R. T.; Shitumbanuma, V.; O'Toole, A.; Sundqvist, K. L.; Arp, H. P. H.; Cornelissen, G. Quantifying the total and bioavailable polycyclic aromatic hydrocarbons and dioxins in biochars. *Environ. Sci. Technol.* **2012**, *46*, 2830−2838.

(24) Woolf, D.; Amonette, J. E.; Street-Perrott, F. A.; Lehmann, J.; Joseph, S. Sustainable biochar to mitigate global climate change. *Nat. Commun.* **2010**, *1*, 56.

(25) Liu, W.-J.; Li, W.-W.; Jiang, H.; Yu, H.-Q. Fates of Chemical Elements in Biomass during Its Pyrolysis. *Chem. Rev.* **2017**, *117*, 6367−6398.

(26) Meyer, S.; Glaser, B.; Quicker, P. Technical, economical, and climate-related aspects of biochar production technologies: A literature review. *Environ. Sci. Technol.* **2011**, *45*, 9473−9483.

(27) Liu, W.-J.; Tian, K.; Jiang, H.; Yu, H.-Q. Facile synthesis of highly efficient and recyclable magnetic solid acid from biomass waste. *Sci. Rep.* **2013**, *3*, 2419.

(28) Thompson, K. A.; Shimabuku, K. K.; Kearns, J. P.; Knappe, D. R. U.; Summers, R. S.; Cook, S. M. Environmental Comparison of Biochar and Activated Carbon for Tertiary Wastewater Treatment. *Environ. Sci. Technol.* **2016**, *50*, 11253−11262.

DOI: 10.1021/acsomega.7b01386
ACS Omega 2017, 2, 7730−7738

(29) Jung, D. S.; Ryou, M.-H.; Sung, Y. J.; Park, S. B.; Choi, J. W. Recycling rice husks for high-capacity lithium battery anodes. *Proc. Natl. Acad. Sci. U.S.A.* **2013**, *110*, 12229−12234.
(30) Qian, L.; Chen, B. Interactions of aluminum with biochars and oxidized biochars: Implications for the biochar aging process. *J. Agric. Food Chem.* **2014**, *62*, 373−380.
(31) Ling, L.-L.; Liu, W.-J.; Zhang, S.; Jiang, H. Magnesium Oxide Embedded Nitrogen Self-Doped Biochar Composites: Fast and High-Efficiency Adsorption of Heavy Metals in an Aqueous Solution. *Environ. Sci. Technol.* **2017**, *51*, 10081−10089.
(32) Shimabuku, K. K.; Kearns, J. P.; Martinez, J. E.; Mahoney, R. B.; Moreno-Vasquez, L.; Summers, R. S. Biochar sorbents for sulfamethoxazole removal from surface water, stormwater, and wastewater effluent. *Water Res.* **2016**, *96*, 236−245.
(33) Zhao, L.; Cao, X.; Zheng, W.; Scott, J. W.; Sharma, B. K.; Chen, X. Copyrolysis of Biomass with Phosphate Fertilizers To Improve Biochar Carbon Retention, Slow Nutrient Release, and Stabilize Heavy Metals in Soil. *ACS Sustainable Chem. Eng.* **2016**, *4*, 1630−1636.
(34) Wu, Y.; Zhang, P.; Zeng, G.; Ye, J.; Zhang, H.; Fang, W.; Liu, J. Enhancing Sewage Sludge Dewaterability by a Skeleton Builder: Biochar Produced from Sludge Cake Conditioned with Rice Husk Flour and FeCl3. *ACS Sustainable Chem. Eng.* **2016**, *4*, 5711−5717.
(35) Saquing, J. M.; Yu, Y.-H.; Chiu, P. C. Wood-Derived Black Carbon (Biochar) as a Microbial Electron Donor and Acceptor. *Environ. Sci. Technol. Lett.* **2016**, *3*, 62−66.
(36) Shimabuku, K. K.; Paige, J. M.; Luna-Aguero, M.; Summers, R. S. Simplified Modeling of Organic Contaminant Adsorption by Activated Carbon and Biochar in the Presence of Dissolved Organic Matter and Other Competing Adsorbates. *Environ. Sci. Technol.* **2017**, *51*, 10031−10040.
(37) Johari, K.; Saman, N.; Song, S. T.; Cheu, S. C.; Kong, H.; Mat, H. Development of coconut pith chars towards high elemental mercury adsorption performance—Effect of pyrolysis temperatures. *Chemosphere* **2016**, *156*, 56−68.
(38) Bala, T.; Prasad, B. L. V.; Sastry, M.; Kahaly, M. U.; Waghmare, U. V. Interaction of Different Metal Ions with Carboxylic Acid Group: A Quantitative Study. *J. Phys. Chem. A* **2007**, *111*, 6183−6190.
(39) Mehandzhiyski, A. Y.; Riccardi, E.; vanErp, T. S.; Koch, H.; Åstrand, P.-O.; Trinh, T. T.; Grimes, B. A. Density Functional Theory Study on the Interactions of Metal Ions with Long Chain Deprotonated Carboxylic Acids. *J. Phys. Chem. A* **2015**, *119*, 10195−10203.
(40) Smith, B. B.; Betts, R. H. Structure and Stereochemistry of a Cobalt(III)-Diethylenetriaminepentaacetic Acid Complex. *J. Am. Chem. Soc.* **1969**, *91*, 7749−7751.
(41) Wicklund, P. A.; Brown, D. G. Synthesis and characterization of some cobalt(III) catechol complexes. *Inorg. Chem.* **1976**, *15*, 396−400.
(42) Gajski, G.; Garaj-Vrhovac, V. Melittin: A lytic peptide with anticancer properties. *Environ. Toxicol. Pharmacol.* **2013**, *36*, 697−705.
(43) Adade, C. M.; Oliveira, I. R. S.; Pais, J. A. R.; Souto-Padrón, T. Melittin peptide kills Trypanosoma cruzi parasites by inducing different cell death pathways. *Toxicon* **2013**, *69*, 227−239.
(44) Pramanik, A.; Vangara, A.; Nellore, B.P. V.; Sinha, S.S.; Chavva, S.R.; Jones, S.; Ray, P.C. Development of Multifunctional Fluorescent−Magnetic Nanoprobes for Selective Capturing and Multicolor Imaging of Heterogeneous Circulating Tumor Cells. *ACS Appl. Mater. Interfaces* **2016**, *8*, 15076−15085.
(45) Fan, Z.; Shelton, M.; Singh, A. K.; Senapati, D.; Khan, S. A.; Ray, P. C. Multifunctional Plasmonic Shell−Magnetic Core Nanoparticles for Targeted Diagnostics, Isolation, and Photothermal Destruction of Tumor Cells. *ACS Nano* **2012**, *6*, 1065−1073.
(46) Nellore, B. P. V.; Kanchanapally, R.; Pedraza, F.; Sinha, S. S.; Pramanik, A.; Hamme, A. T.; Arslan, Z.; Sardar, D.; Ray, P. C. Bio-Conjugated Cnt-Bridged 3d Porous Graphene Oxide Membrane for Highly Efficient Disinfection of Pathogenic Bacteria and Removal of Toxic Metals from Water. *ACS Appl. Mater. Interfaces* **2015**, *7*, 19210−19218.
(47) Pramanik, A.; Fan, Z.; Chavva, S. R.; Sinha, S. S.; Ray, P. C. Highly Efficient and Excitation Tunable Two-Photon Luminescence Platform For Targeted Multi-Color MDRB Imaging Using Graphene Oxide. *Sci. Rep.* **2014**, *4*, 6090.
(48) Kanchanapally, R.; Nellore, B. P. V.; Sinha, S. S.; Pedraza, F.; Jones, S. J.; Pramanik, A.; Chavva, S. R.; Tchounwou, C.; Shi, Y.; Vangara, A.; Sardar, D.; Ray, P. C. Antimicrobial Peptide-Conjugated Graphene Oxide Membrane for Efficient Removal and Effective Killing of Multiple Drug Resistant Bacteria. *RSC Adv.* **2015**, *5*, 18881−18887.
(49) Boyce, J. M.; Pop, O.-F.; Abreu-Lanfranco, O.; Hung, W. Y.; Fisher, A.; Karjoo, A.; Thompson, B.; Protopapas, Z. A trial of discontinuation of empiric vancomycin therapy in patients with suspected methicillin-resistant Staphylococcus aureus health care-associated pneumonia. *Antimicrob. Agents Chemother.* **2013**, *57*, 1163−1168.
(50) Qadri, S. M. H.; Ueno, Y.; Imambaccus, H.; Almodovar, E. Rapid detection of methicillin-resistant *Staphylococcus aureus* by Crystal MRSA ID System. *J. Clin. Microbiol.* **1994**, *32*, 1830−1832.

DOI: 10.1021/acsomega.7b01386
ACS Omega 2017, 2, 7730−7738